Power Factor Analysis of Flux Modulated Dual-PM Excited Machines based on PM and Armature Flux Linkages

Hong Chen, *Member, IEEE,* Yao Meng, *Member, IEEE,* Boyi Li, Dawei Li, *Senior Member, IEEE,* and Ronghai Qu, *Fellow, IEEE*

***Abstract*—Flux modulated dual-permanent magnet (PM) excited machine (FMDPMM) has become a promising candidate for direct-drive applications, featuring high torque density and efficiency. However, it usually suffers from a low power factor (PF) due to the imbalanced PM and armature flux linkages, which are mainly caused by the abundant PM and armature field harmonics. To address the problem, a comprehensive PF analysis of FMDPMM is conducted in this paper based on PM and armature flux linkages. First, the dominant PM and armature field harmonics contributing to the corresponding flux linkages are investigated using a simplified magnetomotive force (MMF)-permeance model. Based on the qualitative analysis, several practical design guidelines are presented to improve the PF of FMDPMM. Then, the dominant field harmonics and flux linkage contributions of two FMDPMMs with different PM arrangements and winding configurations are comparatively analyzed, quantitatively verifying the effectiveness of the proposed guidelines for PF improvement. The results demonstrate that, by taking advantage of high PM flux linkage, low non-working armature flux linkage, and proper filtering effect of armature windings, MDPMM can simultaneously achieve a high PF and a large torque density. Finally, a prototype is manufactured for validation.**

***Index Terms*—Dual-permanent magnet (PM) excitation, Flux modulated machine, Power factor (PF), Flux linkage.**

I. INTRODUCTION

DUE to the high efficiency and reliability, direct-drive permanent magnet (PM) machines (DDPMMs) have been favored in many industrial fields such as wind power plants, electric vehicles, and coal mine tunneling robots [1]-[3]. As a type of DDPMM, the flux modulated PM machine (FMPMM) has attracted increasing attention due to its unique flux modulation mechanism [4]-[7]. FMPMMs can modulate the airgap magnetic field through stator/rotor slotting or special structure designs, resulting in superior performance in terms of torque and power density. Up to now, FMPMMs with various topologies have been proposed [8]-[9]. Based on the placement of PMs, FMPMMs can generally be classified into three categories: flux modulated rotor-PM excited machines (FMRPMMs), flux modulated stator-PM excited machines (FMSPMMs), and flux modulated dual-PM excited machines (FMDPMMs).

Similar to the conventional PM machines, FMRPMMs install PMs on the rotor side, but their stator can be designed with different structures, e.g., open slot [10]-[11], split teeth [12]-[13], hybrid arrangement teeth [14], and segmented stator [15]. In addition, the rotor-PMs of FMRPMMs can also be designed with different types. In [16], four vernier PM machines with different rotor-PM arrangements are compared. In [17], the power factor (PF) characteristic of a vernier machine with V-/I-shaped rotor-PMs is comprehensively analyzed. Apart from FMRPMM, FMSPMM is also a critical category of FMPMMs [18]-[22]. Compared to FMRPMMs, FMSPMMs with PMs equipped in the stator have the merit of easy heat dissipation. In addition, their rotors can be designed with a salient pole structure without PMs, which simplifies the manufacturing process and enhances mechanical reliability.

The emerging FMDPMMs with PMs on both the stator and rotor can utilize the bidirectional flux modulation effect [23]-[26] to transmit much higher torque density than the other two types of machines, which has attracted more and more attention in the last decade. In [27], two FMDPMMs with different stator-PM arrangements are proposed and compared, which shows that the FMDPMM with "N-Fe-N-Fe" arrangement offers higher torque density and efficiency, but a lower PF than the one with "N-Fe-Fe-N" arrangement due to its larger inductance. In [28], four FMDPMMs with different topologies are comprehensively compared to show their advantages based on finite element analysis (FEA). In [29], a linear FMDPMM is presented to generate additional working harmonics through asymmetric design, improving thrust density and reducing PM material usage significantly. In addition, an FMDPMM with asymmetric consequent-pole PM arrangement is proposed to reduce flux leakage and enhance

Manuscript received January 03, 2026; revised February 23, 2026; accepted March 04, 2026. Date of publication June 25, 2026. Date of current version April 03, 2026.

This work was supported by the National Natural Science Foundation of China under Grant 52404171.

Hong Chen, Yao Meng, and Boyi Li are with the College of Electrical Engineering and Automation, Shandong University of Science and Technology, Qingdao 266590, China (e-mail: hongchen@sdust.edu.cn; mengyqd@163.com; byli_sdust@163.com).

Dawei Li and Ronghai Qu are with the School of Electrical and Electronic Engineering, Huazhong University of Science and Technology, Wuhan 430074, China (e-mail: daweili@hust.edu.cn; ronghaiqu@hust.edu.cn).

(*Corresponding author*: *Yao Meng*)

Digital Object Identifier 10.30941/CESTEMS.2026.00011

PF attributed to low non-working armature harmonics [30]-[31]. In [32], a fault-tolerant FMDPMM is developed employing hybrid stator designs, which proves to have good fault tolerance and improved torque density and PF. Moreover, the spoke-type PMs [33] and Halbach-array PMs [34] have been employed in the stator slots of FMDPMMs, which can contribute to improved torque density and PF. In [35], the torque generation mechanism of FMDPMM is analyzed based on airgap field modulation theory. Although scholars have conducted extensive research on FMDPMMs, particularly in aspects such as the design of new topologies and the generation mechanisms of back-electromotive force (back-EMF) and torque, there is a lack of underlying mechanism analysis of their PF characteristics and general design guidelines for achieving a high-PF in FMDPMMs.

To address this problem, this paper aims to analyze the PF of FMDPMM based on PM and armature flux linkages, and to provide design guidelines for PF enhancement via harmonic-level regulation of these flux linkages. In Section II, the PF formation mechanism is analyzed. The dominant PM and armature field harmonics contributing to their corresponding flux linkages are identified using a simplified magnetomotive force (MMF)-permeance model. Based on the qualitative analysis, several design guidelines are proposed to improve the PF of FMDPMMs. In Section III, to quantitatively verify the effectiveness of these guidelines, the PFs of two FMDPMMs with different PM arrangements, together with their flux linkage components contributed by the corresponding field harmonics, are comparatively investigated. Then, in Section IV, a prototype machine is manufactured and tested to verify the FE analysis results. Finally, conclusions are drawn in Section V.

II. Analysis of PF and Flux Linkages

A. PF Formation Mechanism

The PF formation mechanism of FMDPMM is illustrated in Fig. 1, in which consequent-pole PMs and salient iron poles are arranged on both the stator and rotor sides. According to the principle of flux modulation, the stator-PM MMF produced by the stator-PMs interacts with the rotor iron poles, generating a stator-PM field rich in spatial harmonics. Similarly, the rotor-PM magnetic field with abundant harmonics is generated through the interaction between the rotor-PM MMF and the stator iron poles. Meanwhile, the armature windings carrying alternating currents produce an initial armature MMF, which is further modulated by both the stator and rotor iron poles, resulting in a multi-harmonic armature magnetic field. Subsequently, through the filtering effect of the armature windings, the effective PM and armature field harmonics are selected to generate the PM and armature flux linkages. These flux linkage components are directly related to the PF and output torque of FMDPMM, thereby establishing a direct relationship between the field harmonics and the PF.

The phasor diagram of FMDPMM is depicted in Fig. 1, where ψ_{ps} and ψ_{pr} denote the flux linkages produced by stator-PMs and rotor-PMs, respectively. ψ_a is the armature flux linkage, and ψ_σ is the leakage flux. E_{ph} and U_{ph} are the phase back-EMF and voltage, respectively. ω represents the electric angular velocity, and φ is the PF angle. With zero d-axis current control and negligible winding resistance, the PF of FMDPMM is expressed as:

$$\mathrm{PF}=\cos\varphi=\left[1+\left(\frac{\psi_a+\psi_\sigma}{\psi_{ps}+\psi_{pr}}\right)^2\right]^{-\frac{1}{2}} \tag{1}$$

According to (1), the PF is fundamentally determined by the magnitudes of the PM and armature flux linkages. For a fixed ψ_a, increasing either ψ_{ps} or ψ_{pr} can enhance both the PF and torque of FMDPMM. Conversely, reducing ψ_a can enlarge the PF but may lead to a decrease in torque. To achieve simultaneous improvement in PF and torque of FMDPMM, it is essential to decompose these resultant flux linkages into their constituent field harmonic components and identify the dominant harmonic contributions from both the PM and armature excitations.

B. PM Flux Linkage

The PM flux linkage of FMDPMM is produced by the synthetic PM magnetic field jointly excited by the stator-PM MMF $F_{ps}(\theta)$ and rotor-PM MMF $F_{pr}(\theta)$, which can be expressed as follows, respectively:

$$F_{ps}(\theta)=\sum_{m=1}^{\infty}F_{psm}\cos\left(mN_{sp}\theta\right) \tag{2}$$

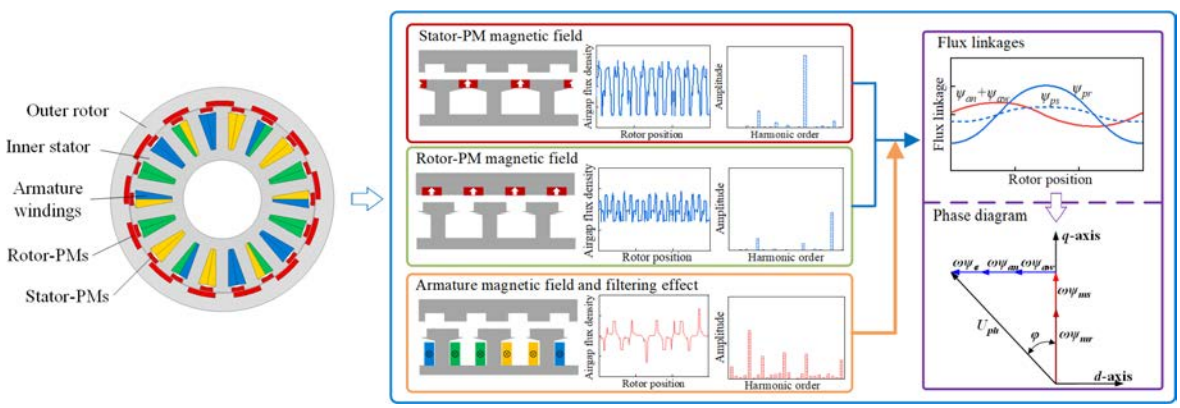

Fig. 1. PF formation mechanism of FMDPMM.

$$F_{\mathrm{pr}}(\theta,t)=\sum_{n=1}^{\infty}F_{\mathrm{pr}n}\cos\left[nN_{\mathrm{r}}(\theta-\Omega_{\mathrm{r}}t)\right] \tag{3}$$

where $F_{\mathrm{ps}m}$ and $F_{\mathrm{pr}n}$ denote the amplitudes of the mth and nth harmonics of the stator-PM and rotor-PM MMFs, respectively. N_{sp} and N_{r} are the stator-PM and rotor-PM pole pair numbers, respectively. θ is the rotor position reference to the stator, Ω_{r} is the mechanical angular velocity, and t is the time. Due to the doubly-salient airgap structure of FMDPMM, the stator permeance function $\Lambda_{\mathrm{s}}(\theta)$ and rotor permeance function $\Lambda_{\mathrm{r}}(\theta, t)$ can be expressed as follows, respectively:

$$\Lambda_{\mathrm{s}}(\theta)=\Lambda_{\mathrm{s}0}+\sum_{i=1}^{\infty}\Lambda_{\mathrm{s}i}\cos\left(iN_{\mathrm{sp}}\theta\right) \tag{4}$$

$$\Lambda_{\mathrm{r}}(\theta,t)=\Lambda_{\mathrm{r}0}+\sum_{j=1}^{\infty}\Lambda_{\mathrm{r}j}\cos\left[jN_{\mathrm{r}}(\theta-\Omega_{\mathrm{r}}t)\right] \tag{5}$$

where $\Lambda_{\mathrm{s}0}$ and $\Lambda_{\mathrm{r}0}$ represent DC components of the stator and rotor permeances, respectively, while $\Lambda_{\mathrm{s}i}$ and $\Lambda_{\mathrm{r}j}$ denote the amplitudes of the ith and jth harmonics of the respective permeance. According to the bidirectional flux modulation theory, the synthetic flux density $B_{\mathrm{p}}(\theta,t)$ produced by the dual-PMs can be obtained as:

$$\begin{aligned}B_{\mathrm{p}}(\theta,t)&=F_{\mathrm{ps}}(\theta)\Lambda_{\mathrm{r}}(\theta,t)+F_{\mathrm{pr}}(\theta,t)\Lambda_{\mathrm{s}}(\theta)\\&=\sum_{m=1}^{\infty}B_{\mathrm{ps}|mN_{\mathrm{sp}}|}\cos\left(mN_{\mathrm{sp}}\theta\right)\\&+\sum_{m=1}^{\infty}\sum_{j=1}^{\infty}B_{\mathrm{ps}|jN_{\mathrm{r}}\pm mN_{\mathrm{sp}}|}\cos\left[\left(jN_{\mathrm{r}}\pm mN_{\mathrm{sp}}\right)\theta-jN_{\mathrm{r}}\Omega_{\mathrm{r}}t\right]\\&+\sum_{n=1}^{\infty}B_{\mathrm{pr}|nN_{\mathrm{r}}|}\cos\left[nN_{\mathrm{r}}(\theta-\Omega_{\mathrm{r}}t)\right]\\&+\sum_{i=1}^{\infty}\sum_{n=1}^{\infty}B_{\mathrm{pr}|nN_{\mathrm{r}}\pm iN_{\mathrm{sp}}|}\cos\left[\left(nN_{\mathrm{r}}\pm iN_{\mathrm{sp}}\right)\theta-nN_{\mathrm{r}}\Omega_{\mathrm{r}}t\right]\end{aligned} \tag{6}$$

where $B_{\mathrm{ps}|mN_{\mathrm{sp}}|}$ and $B_{\mathrm{ps}|jN_{\mathrm{r}}\pm mN_{\mathrm{sp}}|}$ are the amplitudes of the mN_{sp}-th and $|jN_{\mathrm{r}}\pm mN_{\mathrm{sp}}|$-th flux density harmonics produced by the stator-PMs, respectively. $B_{\mathrm{pr}|nN_{\mathrm{r}}|}$ and $B_{\mathrm{pr}|nN_{\mathrm{r}}\pm iN_{\mathrm{sp}}|}$ are the amplitudes of the nN_{r}-th and $|nN_{\mathrm{r}}\pm iN_{\mathrm{sp}}|$-th harmonics produced by the rotor-PMs, respectively. According to (6), it can be seen that besides the stationary harmonics, the PM magnetic field consists of the $|jN_{\mathrm{r}}\pm mN_{\mathrm{sp}}|$-th, nN_{r}-th, and $|nN_{\mathrm{r}}\pm iN_{\mathrm{sp}}|$-th rotating harmonics.

Then the PM flux linkage $\psi_{\mathrm{p}}(t)$ can be derived and expressed as:

$$\begin{cases}\psi_{\mathrm{p}}(t)=r_{\mathrm{g}}l_{\mathrm{st}}\int_0^{2\pi}B_{\mathrm{p}}(\theta,t)N(\theta)\,\mathrm{d}\theta=\psi_{\mathrm{ps}}(t)+\psi_{\mathrm{pr}}(t)\\N(\theta)=\sum_{h=1}^{\infty}\dfrac{2}{h\pi}N_{\mathrm{t}}k_{wh}\cos(h\theta)\end{cases} \tag{7}$$

where $N(\theta)$ represents the winding function, r_{g} is the airgap radius, and l_{st} is the active stack length. N_{t} is the turns in series per phase. k_{wh} is the winding factor of the h-th harmonic. $\psi_{\mathrm{ps}}(t)$ and $\psi_{\mathrm{pr}}(t)$ are the flux linkage produced by stator-PMs and rotor-PMs, respectively, which can be expressed as (8) and (9):

$$\psi_{\mathrm{ps}}(t)=C_0\sum_{m=1}^{\infty}\sum_{j=1}^{\infty}B_{\mathrm{ps}|jN_{\mathrm{r}}\pm mN_{\mathrm{sp}}|}\frac{k_{\mathrm{w}|jN_{\mathrm{r}}\pm mN_{\mathrm{sp}}|}}{|jN_{\mathrm{r}}\pm mN_{\mathrm{sp}}|}\cos jN_{\mathrm{r}}\Omega_{\mathrm{r}}t \tag{8}$$

$$\begin{aligned}\psi_{\mathrm{pr}}(t)&=C_0\sum_{n=1}^{\infty}B_{\mathrm{pr}|nN_{\mathrm{r}}|}\frac{k_{\mathrm{w}nN_{\mathrm{r}}}}{nN_{\mathrm{r}}}\cos nN_{\mathrm{r}}\Omega_{\mathrm{r}}t\\&+C_0\sum_{n=1}^{\infty}\sum_{n=1}^{\infty}B_{\mathrm{pr}|nN_{\mathrm{r}}\pm iN_{\mathrm{sp}}|}\frac{k_{\mathrm{w}|nN_{\mathrm{r}}\pm iN_{\mathrm{sp}}|}}{|nN_{\mathrm{r}}\pm iN_{\mathrm{sp}}|}\cos nN_{\mathrm{r}}\Omega_{\mathrm{r}}t\end{aligned} \tag{9}$$

where $C_0 = 2r_{\mathrm{g}}l_{\mathrm{st}}N_{\mathrm{t}}$. Since only the fundamental PM flux linkage contributes to generating the steady output torque, the j and n in (8) and (9) equal 1. Consequently, the dominant working PM field harmonics contain the $|N_{\mathrm{r}}\pm mN_{\mathrm{sp}}|$-th, N_{r}-th, and $|N_{\mathrm{r}}\pm iN_{\mathrm{sp}}|$-th orders. The PM flux linkage components of FMDPMM and their contributing field harmonics are summarized in Table I. Accordingly, it can be observed that the PM flux linkages ψ_{ps} and ψ_{pr} are both directly impacted by the amplitudes of both the stator and rotor-PM dominant flux density harmonics and corresponding winding factors with the same harmonic orders.

TABLE I
PM FLUX LINKAGE COMPONENTS OF FMDPMM

Item	Source	Amplitude	Contributing field harmonic
ψ_{ps}	Stator-PMs	$C_0\sum_{m=1}^{\infty}B_{\mathrm{ps}\lvert N_{\mathrm{r}}\pm mN_{\mathrm{sp}}\rvert}\frac{k_{\mathrm{w}\lvert N_{\mathrm{r}}\pm mN_{\mathrm{sp}}\rvert}}{\lvert N_{\mathrm{r}}\pm mN_{\mathrm{sp}}\rvert}$	$\lvert N_{\mathrm{r}}\pm mN_{\mathrm{sp}}\rvert$
		$C_0B_{\mathrm{pr}\lvert N_{\mathrm{r}}\rvert}\frac{k_{\mathrm{w}N_{\mathrm{r}}}}{N_{\mathrm{r}}}$	N_{r}
ψ_{pr}	Rotor-PMs	$C_0\sum_{i=1}^{\infty}B_{\mathrm{pr}\lvert N_{\mathrm{r}}\pm iN_{\mathrm{sp}}\rvert}\frac{k_{\mathrm{w}\lvert N_{\mathrm{r}}\pm iN_{\mathrm{sp}}\rvert}}{\lvert N_{\mathrm{r}}\pm iN_{\mathrm{sp}}\rvert}$	$\lvert N_{\mathrm{r}}\pm iN_{\mathrm{sp}}\rvert$

C. Armature Flux Linkage

The armature MMF $F_{\mathrm{a}}(\theta, t)$ can be expressed as:

$$F_{\mathrm{a}}(\theta,t)=\sum_{v=1}^{\infty}F_{\mathrm{a}v}\cos\left[v\theta-\mathrm{sgn}(v)N_{\mathrm{r}}\Omega_{\mathrm{r}}t\right] \tag{10}$$

where $F_{\mathrm{a}v} = 3N_{\mathrm{t}}I_{\mathrm{m}}k_{wv}/(v\pi)$ represents the amplitude of the vth armature MMF harmonic. I_{m} is the current amplitude, and k_{wv} is the winding factor of the vth harmonic. sgn(v) is the sign function to reflect the rotation direction of the vth harmonic. Then the airgap flux density produced by the armature MMF $B_{\mathrm{a}}(\theta, t)$ can be expressed as:

$$\begin{aligned}B_{\mathrm{a}}(\theta,t)&=\frac{\mu_0}{g}F_{\mathrm{a}}(\theta,t)\Lambda_{\mathrm{s}}(\theta)\Lambda_{\mathrm{r}}(\theta,t)\\&=\sum_{v=1}^{\infty}B_{\mathrm{a}v}\cos\left[v\theta-\mathrm{sgn}(v)N_{\mathrm{r}}\Omega_{\mathrm{r}}t\right]\\&+\sum_{v=1}^{\infty}\sum_{j=1}^{\infty}B_{\mathrm{a}|v\pm jN_{\mathrm{r}}|}\cos\left\{\left(v\pm jN_{\mathrm{r}}\right)\theta-\left[\mathrm{sgn}(v)\pm j\right]N_{\mathrm{r}}\Omega_{\mathrm{r}}t\right\}\\&+\sum_{v=1}^{\infty}\sum_{i=1}^{\infty}B_{\mathrm{a}|v\pm iN_{\mathrm{sp}}|}\cos\left[\left(v\pm iN_{\mathrm{sp}}\right)\theta-\mathrm{sgn}(v)N_{\mathrm{r}}\Omega_{\mathrm{r}}t\right]\\&+\sum_{v=1}^{\infty}\sum_{i=1}^{\infty}\sum_{j=1}^{\infty}B_{\mathrm{a}|jN_{\mathrm{r}}\pm iN_{\mathrm{sp}}\pm v|}\cos\begin{Bmatrix}\left(jN_{\mathrm{r}}\pm iN_{\mathrm{sp}}\pm v\right)\theta\\-\left[j\pm\mathrm{sgn}(v)\right]N_{\mathrm{r}}\Omega_{\mathrm{r}}t\end{Bmatrix}\end{aligned} \tag{11}$$

where μ_0 and g are the vacuum permeability and airgap length, respectively. $B_{\mathrm{a}v}$, $B_{\mathrm{a}|v\pm jN_{\mathrm{r}}|}$, $B_{\mathrm{a}|v\pm iN_{\mathrm{sp}}|}$, and $B_{\mathrm{a}|jN_{\mathrm{r}}\pm iN_{\mathrm{sp}}\pm v|}$ are the amplitudes of the corresponding flux density harmonics produced by armature windings, respectively. From (11), it can be observed that the armature magnetic field

of FMDPMM can provide the harmonics including the v-th, $|v\pm jN_r|$-th, $|v\pm iN_{sp}|$-th, and $|jN_r\pm iN_{sp}\pm v|$-th orders.

The expression of the fundamental armature flux linkage $\psi_a(t)$ can be derived by:

$$\begin{aligned}\psi_a(t) &= r_g l_{st}\int_0^{2\pi} B_a(\theta,t)N(\theta)\,\mathrm{d}\theta \\ &= C_0\sum_{v=1}^{\infty} B_{av}\frac{k_{wv}}{v}\cos N_r\Omega_r t \\ &+C_0\sum_{v=2,5,8..}^{\infty} B_{a|v\pm 2N_r|}\frac{k_{w|v\pm 2N_r|}}{|v\pm 2N_r|}\cos N_r\Omega_r t \\ &+C_0\sum_{v=1}^{\infty}\sum_{i=1}^{\infty} B_{a|v\pm iN_{sp}|}\frac{k_{w|v\pm iN_{sp}|}}{|v\pm iN_{sp}|}\cos N_r\Omega_r t \\ &+C_0\sum_{v=2,5,8..}^{\infty}\sum_{i=1}^{\infty} B_{a|2N_r\pm iN_{sp}\pm v|}\frac{k_{w|2N_r\pm iN_{sp}\pm v|}}{|2N_r\pm iN_{sp}\pm v|}\cos N_r\Omega_r t\end{aligned} \tag{12}$$

It can be found that the dominant armature field harmonics contributed to the armature flux linkage are the v-th, $|v\pm 2N_r|$-th, $|v\pm iN_{sp}|$-th, and $|2N_r\pm iN_{sp}\pm v|$-th orders. The armature flux linkage components of FMDPMM and their contributing field harmonics are listed in Table II.

TABLE II
ARMATURE FLUX LINKAGE COMPONENTS OF FMDPMM

Item	Amplitude	Contributing field harmonic
ψ_a	$C_0\sum_{v=1}^{\infty} B_{av}\frac{k_{wv}}{v}$	v
	$C_0\sum_{v=2,5,8,...}^{\infty} B_{a\|v\pm 2N_r\|}\frac{k_{w\|v\pm 2N_r\|}}{\|v\pm 2N_r\|}$	$\|v\pm 2N_r\|$
	$C_0\sum_{v=1}^{\infty}\sum_{i=1}^{\infty} B_{a\|v\pm iN_{sp}\|}\frac{k_{w\|v\pm iN_{sp}\|}}{\|v\pm iN_{sp}\|}$	$\|v\pm iN_{sp}\|$
	$C_0\sum_{v=2,5,8,...}^{\infty}\sum_{i=1}^{\infty} B_{a\|2N_r\pm iN_{sp}\pm v\|}\frac{k_{w\|2N_r\pm iN_{sp}\pm v\|}}{\|2N_r\pm iN_{sp}\pm v\|}$	$\|2N_r\pm iN_{sp}\pm v\|$

It should be noted that only the armature field harmonics whose orders are equal to those of the PM field harmonics can produce the steady torque. These harmonics are defined as the working harmonics and generate the working flux linkage ψ_{aw}. The remaining harmonics are referred to as non-working harmonics and produce the non-working flux linkage ψ_{an} [15]. A reduction in ψ_{aw} tends to increase the PF but inevitably leads to a decrease in the average torque, whereas a reduction in ψ_{an} contributes to an improved PF without affecting the torque. Therefore, to simultaneously achieve the design objectives of a high PF and large torque, a feasible strategy is to suppress the ψ_{an} component while maintaining or slightly enhancing the ψ_{aw} component.

D. PF Improvement Guidelines

Based on the foregoing analysis, it can be observed that an efficient approach to improving the PF of FMDPMM is to regulate the PM and armature flux linkages appropriately. This can be achieved through the optimal design of the PM and armature field harmonics, as well as the proper selection of the armature winding configuration and slot-pole combination. Consequently, for an FMDPMM with N_s stator slots, N_{sp} stator-PM pole pairs, N_r rotor pole pairs, and P_a winding pole pairs, the following guidelines should be satisfied to obtain a relatively high PF.

1) Enhancement of PM flux linkages ψ_{ps} and ψ_{pr}. Since high PM flux linkage simultaneously improves the PF and average torque, the stator- and rotor-PM flux linkage components ψ_{ps} and ψ_{pr} should be maximized. Accordingly, the amplitudes of the dominant working PM field harmonics, including the $|N_r\pm mN_{sp}|$-th, N_r-th, and $|N_r\pm iN_{sp}|$-th orders, should be enlarged according to (6)–(9).

2) Balanced armature flux linkage ψ_a generation. To achieve a high PF and torque, the amplitudes of the dominant working armature field harmonics producing ψ_{aw} should be increased, including the v-th, $|v\pm 2N_r|$-th, $|v\pm iN_{sp}|$-th, and $|2N_r\pm iN_{sp}\pm v|$-th orders. Meanwhile, the amplitudes of the non-working armature field harmonics contributing to ψ_{an} should be effectively suppressed, particularly the lower-order components that do not coincide with the orders of the working PM field harmonics.

3) Optimal winding configurations and slot-pole combinations with high winding factors. The goal is to take full use of the filtering effect of the armature windings. For the PM field harmonics, the winding factors of the working harmonics should be as large as that of the P_a-th harmonic k_{wPa}. Consequently, the PM harmonic orders $|N_r\pm mN_{sp}|$, N_r, and $|N_r\pm iN_{sp}|$ should satisfy the following relationship:

$$\begin{cases}\left|N_r\pm mN_{sp}\right| = \left|kN_r\pm P_a\right| \\ N_r = \left|kN_r\pm P_a\right| \\ \left|N_r\pm iN_{sp}\right| = \left|kN_r\pm P_a\right|\end{cases} \tag{13}$$

where k = 0, 1, 2, ... Meanwhile, the working armature field harmonic orders that are equal to $|N_r\pm kN_s|$ (i.e., dominant PM field harmonic orders) should also equal $|kN_s\pm P_a|$. In contrast, the non-working armature field harmonic orders should avoid matching $|kN_s\pm P_a|$ to obtain low winding factors. Based on these matching conditions, the effectiveness of a candidate slot-pole combination can be assessed by examining the resulting PM and armature flux linkage spectra, which ultimately leads to an improved PF.

III. FINITE ELEMENT VALIDATION

In this section, two FMDPMMs are developed to validate the effectiveness of the aforementioned analysis, as shown in Fig. 2, named Machine I and Machine II, respectively. Machine I is specifically designed by systematically applying the three guidelines for PF improvement, including employing rich dual-PM field harmonics, low-order armature field harmonics with low amplitudes, and a matching winding configuration that ensures high winding factors for all working PM field harmonics while providing low winding factors for low-order harmonics. Machine II serves as a benchmark for comparison. Both FMDPMMs have 18 stator slots and 13 rotor pole pairs, but differ in their stator-PM arrangements. Based on the flux modulation theory, the stator-PM pole pair number N_{sp} of Machine I equals N_s, while for

Machine II, $N_{sp} = N_s/2$. Therefore, the armature winding pole pairs P_a of the two FMDPMMs are 5 and 4, respectively. To ensure a fair comparative analysis, both machines are globally optimized for maximized torque density and PF under the same design constraints, including rotor outer and inner diameters, airgap and stack lengths, electrical loading, and materials. Key geometric parameters, such as stator tooth widths, PM heights, and pole arcs, are varied using a parametric sweep coupled with FEA. The main parameters are summarized in Table III.

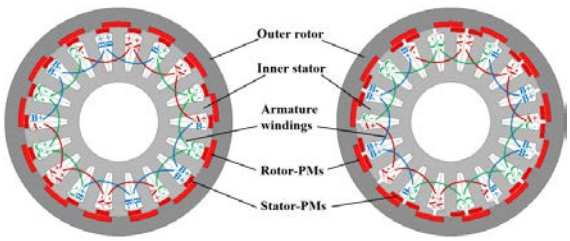

Fig. 2. Machine topologies of the two compared FMDPMMs. (a) Machine I. (b) Machine II.

TABLE III
PARAMETERS OF THE TWO COMPARED FMDPMMS

Parameter	Machine I	Machine II
Stator slot number, N_s	18	
Rotor pole pair, N_r	13	
Winding pole pair, P_a	5	4
Stator-PM pole pair, N_{sp}	18	9
Rotor outer diameter/mm	122.5	
Stator outer diameter/mm	102	
Stack length/mm	60	
Airgap length/mm	0.4	
Stator-PM thickness/mm	2.2	
Rotor-PM thickness/mm	2.7	
Rated speed/(r·min^{-1})	300	
Turns in series per phase	756	
Copper loss/W	95	
Rated current/A	1.5	
Steel material	50WW470	
PM material	40SH	

A. *PM Field Harmonics and Flux Linkages*

Figs. 3 and 4 show the airgap flux density waveforms and harmonics produced by the PM excitations of the two FMDPMMs. For Machine I, the dominant PM field harmonic orders are the 5th ($|N_r$-$N_{sm}|$-th), 13th (N_r-th), 23rd ($|N_r$-$2N_{sm}|$-th), and 31st ($|N_r$+$N_{sm}|$-th), which are produced by both the stator and rotor-PM fields. As for Machine II, it can be found that there are more PM flux field harmonics than those of Machine I. The dominant harmonic components include the 4th ($|N_r$-$N_{sm}|$-th), 5th ($|2N_{sm}$-$N_r|$-th), 9th (N_{sm}-th), 13th (N_r-th), 18th ($2N_{sm}$-th), 22nd ($|N_{sm}$+$N_r|$-th), and 32nd ($|5N_{sm}$-$N_r|$-th) orders. However, with the filtering effect of the armature winding (indicated by the winding factors of $P_a = 4$ in Table IV), only the even order harmonics (4th, 22nd, and 32nd) are the dominant working harmonics for Machine II. Then, the PM flux linkage waveforms and harmonic contributions of the two FMDPMMs are investigated in Figs. 5 and 6. It can be observed that for Machine I, the rotor-PMs produce nearly 80% of the total PM flux linkage. Moreover, the dominant harmonics that contribute positively to the PM flux linkage are the 5th and 13th, while the 23rd and 31st contribute negatively. For Machine II, the dominant harmonics are the 4th and 22nd, while the contribution of the 32nd harmonic is relatively minor. To provide a quantitative perspective, the amplitudes and components of the dominant PM flux harmonics and corresponding contributions to flux linkages of the two FMDPMMs are compared in Table V. Therefore, it can be concluded that the PM field harmonics of Machine I exert a stronger enhancement effect on the PM flux linkages than those of Machine II, owing to a more effective winding filtering effect of Machine I that selectively extracts the working PM field harmonics with larger amplitudes, consistent with guidelines (1) and (3).

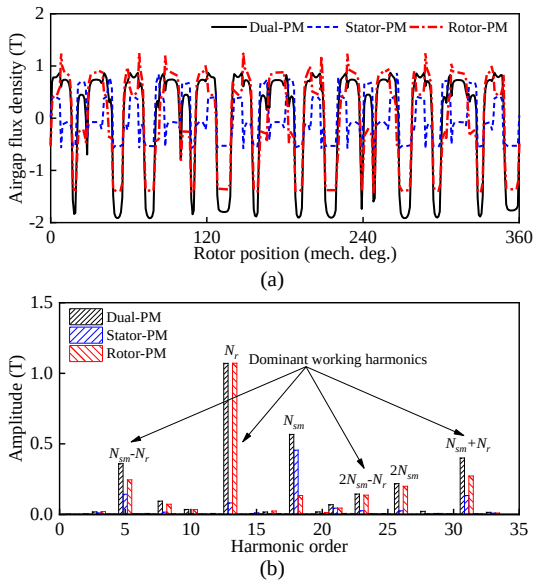

Fig. 3. Airgap flux densities of Machine I produced by PMs. (a) Waveforms. (b) Harmonics.

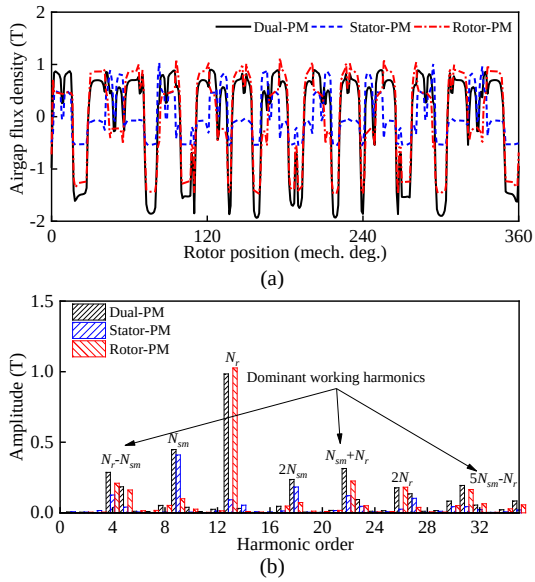

Fig. 4. Airgap flux densities of Machine II produced by PMs. (a) Waveforms. (b) Harmonics.

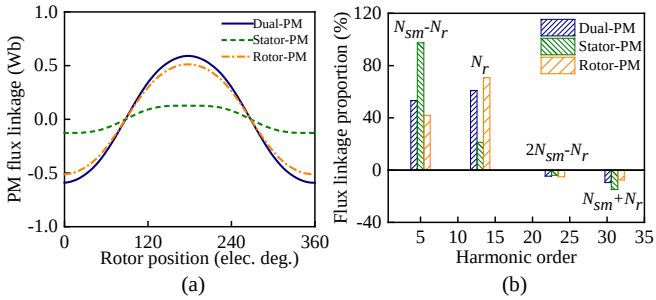

Fig. 5. PM flux linkages of Machine I. (a) Waveforms. (b) Harmonic contributions.

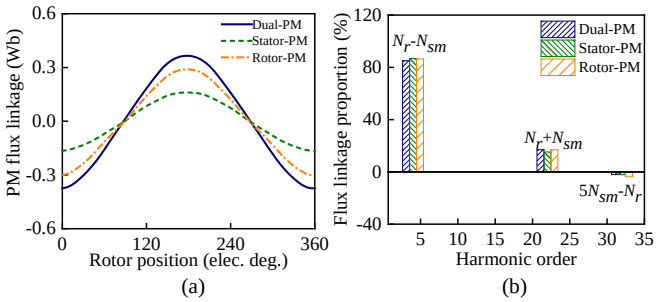

Fig. 6. PM flux linkages of Machine II. (a) Waveforms. (b) Harmonic contributions.

TABLE IV
WINDING FACTORS OF THE 18-SLOT ARMATURE WINDINGS

Item	Winding factor, k_{wk}						
$P_a = 5$	1st	5th	7th	11th	13th	17th	19th
	−0.06	0.95	0.14	−0.14	−0.95	0.06	−0.06
$P_a = 4$	2nd	4th	8th	10th	14th	16th	20th
	−0.14	−0.95	0.06	−0.06	0.95	0.14	−0.14

TABLE V
QUANTITATIVE COMPARISON OF DOMINANT PM HARMONICS AND CORRESPONDING CONTRIBUTIONS

Type	Order, k	Amplitude, T	Proportion/%
Machine I	5th	0.36	53.23
	13th	1.07	60.97
	23rd	0.14	–4.64
	31st	0.40	–9.56
Machine II	4th	0.29	85.07
	22nd	0.31	16.95
	32nd	0.05	–2.03

B. Armature Field Harmonics and Flux Linkages

The primitive armature MMF waveforms and harmonics of the two FMDPMMs are depicted in Fig. 7. It shows that for Machine I, there are only odd-order MMF harmonics and the main MMF harmonics with high amplitudes include the 1st, 5th, 7th, and 13th orders. For Machine II, there are only even-order MMF harmonics and the main harmonic orders are 2nd, 4th, and 14th. Additionally, the winding factors of both armature windings are listed in Table IV, which help to filter the corresponding harmonics.

Then the armature magnetic fields can be produced by the modulating interaction of the armature MMFs and the salient teeth of the stator and rotor. Fig. 8 shows the airgap flux density waveforms and harmonics produced by the armature

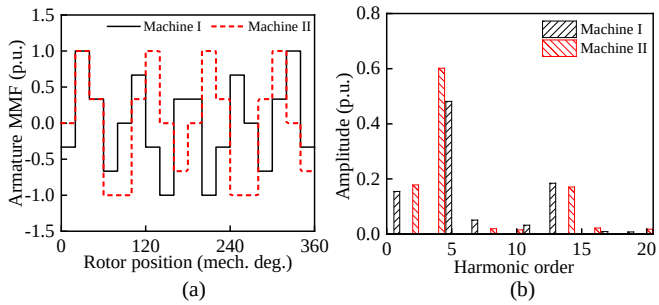

Fig. 7. Armature MMFs of the two FMDPMMs. (a) Waveforms. (b) Harmonics.

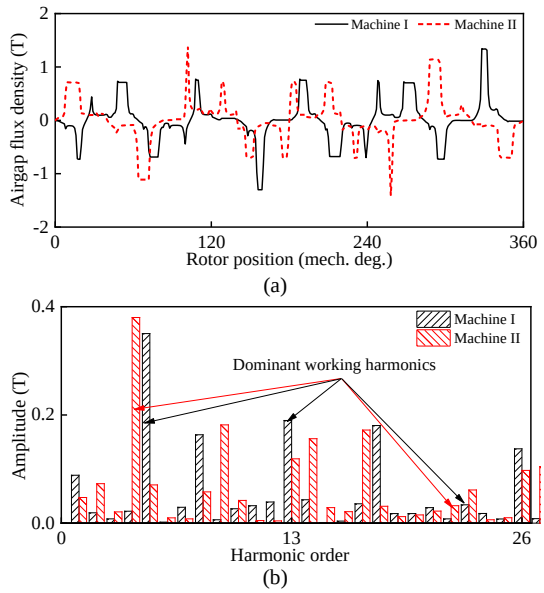

Fig. 8. Armature airgap flux densities of the two FMDPMMs. (a) Waveforms. (b) Harmonics.

MMFs, which are categorized into working and non-working harmonics and detailed in Table VI. In Machine I, the working armature field harmonics comprise the 5th, 13th, 23rd, and 31st orders, whereas the non-working harmonics consist of other odd orders such as the 1st, 7th, 11th, and 17th. In contrast, Machine II exhibits working harmonics at the 4th and 22nd orders, with non-working harmonics including other even orders, such as the 2nd, 8th, 10th, and 14th. Additionally, it can be observed that the dominant working harmonics differ significantly between the two machines, while harmonics of similar orders exhibit comparable amplitudes. Furthermore, the armature flux linkage waveforms and their harmonic contributions of the two FMDPMMs are investigated in Figs. 9 and 10. The results indicate that in Machine I, the dominant working harmonics (5th and 13th) contribute positively to the armature flux linkage, whereas the dominant non-working harmonics (1st and 23rd) exhibit negative contributions. In contrast, both the dominant working and non-working harmonics in Machine II contribute positively to its armature flux linkage, as quantitatively analyzed in Table VII. As a result, although the working harmonics in both machines yield comparable flux linkage components due to their similar amplitudes, the negative contributions from the non-working harmonics in Machine I result in an overall reduction of its

total armature flux linkage. Therefore, the non-working armature field harmonics of Machine I exert a stronger suppressive effect on the armature flux linkage than that of Machine II owing to their negative contributions, which is consistent with guidelines (2) and (3).

TABLE VI
DOMINANT ARMATURE HARMONICS OF THE TWO FMDPMMS

Type	Machine I	Machine II
Working harmonics	5th, 13th, 23rd, and 31st	4th, 22nd, and 32nd
Non-working harmonics	1st, 7th, 11th, 17th,19th, 25th, 29th, …	2nd, 8th, 10th, 14th, 16th, 20th, 26th, 28th, …

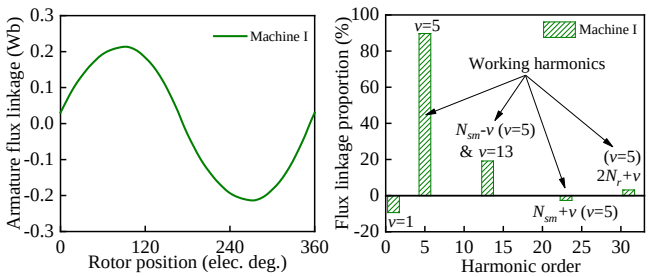

Fig. 9. Armature flux linkages of Machine I. (a) Waveforms. (b) Harmonic contributions.

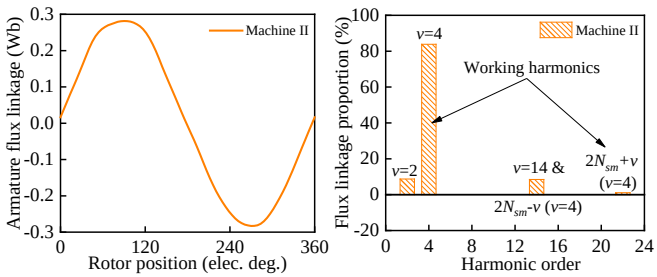

Fig. 10. Armature flux linkages of Machine II. (a) Waveforms. (b) Harmonic contributions.

TABLE VII
QUANTITATIVE COMPARISON OF DOMINANT ARMATURE HARMONICS AND CORRESPONDING CONTRIBUTIONS

Type	Order, k	Amplitude, T	Proportion/%
Machine I	1st	0.09	–9.40
	5th	0.35	89.73
	13th	0.19	19.20
	23rd	0.03	–2.65
	31st	0.07	3.13
Machine II	2nd	0.07	8.55
	4th	0.38	82.05
	14th	0.16	8.31
	22nd	0.03	1.09

C. PF Analysis

The PM and armature flux linkages produced by corresponding field harmonics of the two FRDPMMs are calculated and listed in Table VIII. Additionally, the flux linkage waveforms of the two machines are illustrated in Fig. 11. It shows that Machine I exhibits a lower armature flux linkage and a higher PM flux linkage, compared to Machine II. Based on (1), the PFs of FMDPMMs are calculated and compared in Table VIII. The results show that Machine I can achieve a PF of 0.932, which is 21.5% higher than the value of 0.764 for Machine II. Then, the PFs of the two machines are calculated from the perspective of the PF angle. As investigated in Fig. 12, U_{I} and U_{II} represent fundamental phase voltages of Machine I and Machine II, respectively. I_{ph} is the phase current and is kept the same for the two compared machines. The calculated PF values are 0.938 for Machine I and 0.783 for Machine II, closely matching the values derived from the flux-linkage-based method. Additionally, the curves of the PF values for the two FMDPMMs with varied phase currents are compared in Fig. 13, demonstrating the high-PF priority of Machine I. Furthermore, the torque density of Machine I is 34.2 (N·m)/L, which is 67.9% higher than that of Machine II, as calculated in Table VIII. It can be concluded that, based on the given design guidelines, FMDPMM can achieve a high PF while maintaining a high torque density.

TABLE VIII
PERFORMANCES OF THE TWO FMDPMMS

Parameter	Machine I	Machine II
Armature flux linkage, ψ_{a}/Wb	0.221	0.291
PM flux linkage, ψ_{p}/Wb	0.572	0.345
PF	0.932	0.764
Torque density/(N·m·L^{-1})	34.2	20.37

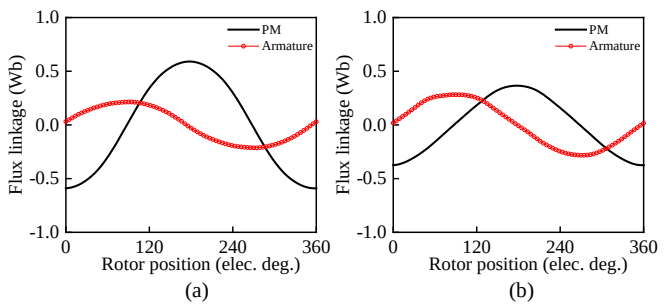

Fig. 11. Flux linkage waveforms of the two FMDPMM. (a) Machine I. (b) Machine II.

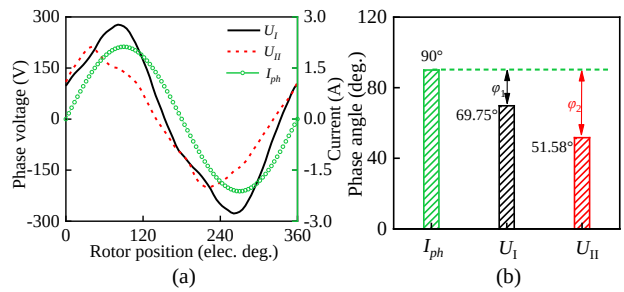

Fig. 12. PF angles of the two FMDPMMs. (a) Waveforms of the phase voltage and current. (b) PF angles.

In summary, compared to Machine II, Machine I exhibits a higher PM flux linkage due to the winding filtering effect that selectively extracts the working PM field harmonics with large amplitudes, and a lower armature flux linkage due to the negative contributions of the non-working armature field harmonics. Consequently, the higher ratio of PM flux linkage to armature flux linkage in Machine I thereby yields a superior PF.

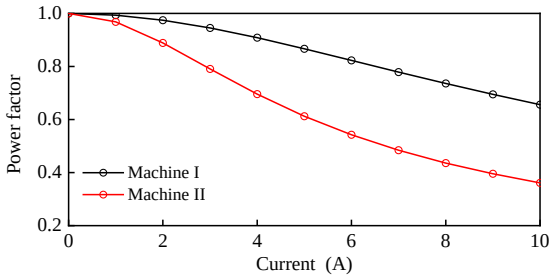

Fig. 13. Curves of the PF values of FMDPMMs with varied phase currents.

IV. Experimental Validation

To verify the foregoing analyses, a prototype of Machine I is manufactured based on the dimensions listed in Table I. The main components of the prototype and the test platform are illustrated in Fig.14.

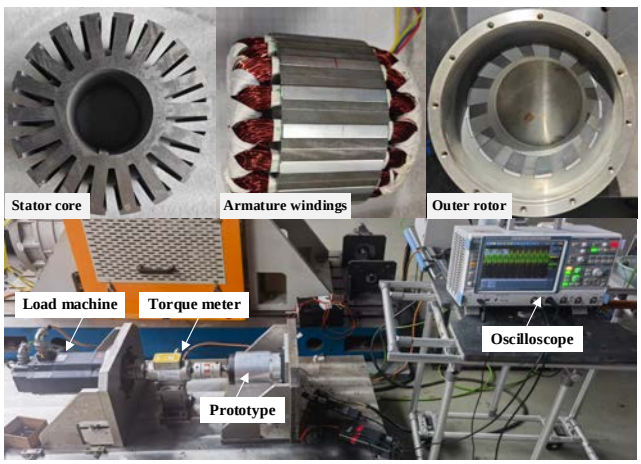

Fig. 14. Prototype and test platform.

The no-load back-EMF of the prototype is measured using an oscilloscope while the rotor is driven at 300 r/min by a servo motor. As shown in Fig. 15(a), the measured and FE-predicted back-EMF waveforms are in good agreement. In Fig. 15(b), the amplitudes of the measured and FE-predicted back-EMFs are 223.3 and 245.5 V, respectively, corresponding to an error of 9.0%, which confirms the accuracy of the FE analysis.

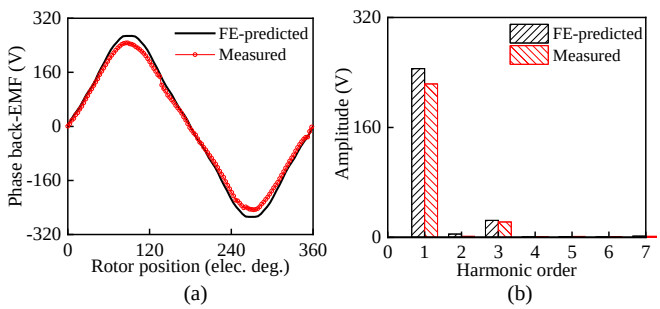

Fig. 15. Open-circuit back-EMF waveforms and harmonics (at 300 r/min). (a) Waveforms. (b) Harmonics.

The torque output capability of the motor is validated by connecting the prototype to a load motor. Dynamic torque measurements are performed at the rated speed of 300 r/min using a torque transducer with a precision of 0.001 N·m. Fig. 16(a) compares the measured and FE-predicted average torque of the prototype under varying currents with the zero d-axis current control strategy. It can be observed that as the current increases from 0 to 5 A, the measured average torques are slightly lower than the FE-predicted values, owing to manufacturing tolerances and end effects. At the rated current of 1.5 A, the measured torque is 21.4 N·m compared to an FE-predicted value of 24.1 N·m. When the current rises to 4.5 A, the measured overload ratio is 2.51, closely matching the FE-predicted ratio of 2.45. Moreover, the PF values at different phase currents are obtained by post-processing the voltage and current waveforms captured by the oscilloscope. The phase difference θ between the fundamental components of voltage and current is extracted via fast Fourier transform (FFT), and the PF is calculated as $\cos(\theta)$. The results are compared with the FE predictions in Fig. 16(b). It can be observed that the results exhibit closely matching trends. At the rated current of 1.5 A, the measured PF reaches 0.932, showing good agreement with the FE-predicted value of 0.94.

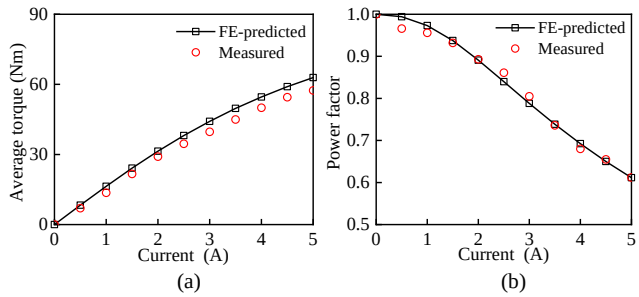

Fig. 16. Curves of average torque and PF with varied phase current. (a) Average torque. (b) PF.

Overall, it can be concluded that the measured results agree well with the FE predictions, demonstrating the effectiveness of the FE analysis.

V. Conclusion

In this paper, the PF analysis of FMDPMMs is comprehensively conducted based on PM and armature flux linkages, and several guidelines for PF improvement are presented. The main conclusions are synthesized as follows.

1) A simplified analytical model of FMDMM is built to reveal that the dominant working harmonics contributing to the PM flux linkage are of the orders $|N_r \pm mN_{sp}|$-th, N_r-th, and $|N_r \pm iN_{sp}|$-th. For the armature flux linkage, the main working harmonics include the v-th, $|v \pm 2N_r|$-th, $|v \pm iN_{sp}|$-th, and $|2N_r \pm iN_{sp} \pm v|$-th orders that coincide with the working PM field harmonics, while the remaining harmonics contribute to the non-working armature flux linkage.

2) Based on this harmonic analysis, design guidelines for PF improvement are established. By appropriately selecting the PM arrangement and armature winding configuration, the dominant PM and armature field harmonics can be effectively enlarged and filtered, thereby increasing the ratio of PM flux linkage to armature flux linkage and resulting in an improved PF.

3) Two FMDPMMs are optimally designed and comparatively evaluated using FEA. The results confirm that Machine I, which benefits from a favorable winding filtering

effect, exhibits a higher PM flux linkage due to the selective extraction of large-amplitude working harmonics. Meanwhile, Machine I also exhibits a lower armature flux linkage owing to the reduced contribution of non-working harmonics.

Finally, a prototype of Machine I is experimentally tested and confirms the effectiveness of the analysis results.

REFERENCES

[1] M. Ghods, J. Faiz, and A. A. Pourmoosa, "Winding Function Model-based Performance Evaluation of a PM Transverse Flux Generator for Applications in Direct-drive Systems," *CES Trans. on Electr. Mach. and Syst.*, vol. 8, no. 2, pp. 216–226, Jun. 2024.

[2] S. F. Jia, P. C. Sun, and S. Feng *et al*., "Analysis and Experiment of a Dual Stator/rotor PM and Winding Flux Modulated PM Machine," *IEEE Trans. on Ind. Appl.*, vol. 59, no. 2, pp. 1659–1669, Mar.-Apr. 2023.

[3] Y. L. Yu, F. Chai, and Y. L. Pei *et al*., "Comparative Study of Loss Characteristic between Permanent Magnet Synchronous Machine and Vernier Machine for In-wheel Direct Drive," *IEEE Trans. on Transp. Electrific.*, vol. 11, no. 1, pp. 2035–2048, Feb. 2025.

[4] M. Cheng, P. Han, and W. Hua, "General Airgap Field Modulation Theory for Electrical Machines," *IEEE Trans. on Ind. Electron.*, vol. 64, no. 8, pp. 6063–6074, Aug. 2017.

[5] Z. X. Li, C. Liu, and Y. W. Fan *et al*., "Analysis and Reduction of Cogging Torque of Permanent Magnet Synchronous Wind Generators based on the Magnetic Field Modulation Mechanism," *CES Trans. on Electr. Mach. and Syst.*, vol. 8, no. 4, pp. 463–470, Dec. 2024.

[6] J. R. Zhou, D. Y. Fan, and Z. X. Xiang *et al*., "Production Mechanism of Power Factor of V-type Vernier Permanent Magnet Machine and Improvement Method," *Trans. of China Electrotech. Soc.*, vol. 38, no. 14, pp. 3789–3799, 2023.

[7] J. W. Chai, X. G. Gui, and Q. Gao *et al*., "Analytical Method of Permanent Magnet Torque Machine with High Torque for Considering the Influence of Armature Magnetic Field," *CES Trans. on Electr. Mach. and Syst.*, vol. 9, no. 3, pp. 289–299, Sept. 2025.

[8] X. H. Zhu, C. H. T. Lee, and C. C. Chan *et al*., "Overview of Flux-modulation Machines based on Flux-modulation Principle: Topology, Theory, and Development Prospects," *IEEE Trans. on Transp. Electrific.*, vol. 6, no. 2, pp. 612–624, Jun. 2020.

[9] Y. Yue, S. F. Jia, and D. L. Liang, "New Topologies of High Torque Density Machine based on Magnetic Field Modulation Principle," *CES Trans. on Electr. Mach. and Syst.*, vol. 7, no. 1, pp. 1–10, Mar. 2023.

[10] A. Toba, and T. A. Lipo, "Generic Torque-maximizing Design Methodology of Surface Permanent-magnet Vernier Machine," *IEEE Trans. on Ind. Appl.*, vol. 36, no. 6, pp. 1539–1546, Nov.-Dec. 2000.

[11] L. B. Cao, Y. F. Zuo, and X. H. Zhu *et al*., "Investigation of Permanent-magnet Vernier Machine with Fractional-slot Nonoverlapping Windings for Direct-drive Application," *IEEE Trans. on Transport. Electrific.*, vol. 10, no. 2, pp. 3383–3395, Jun. 2024.

[12] T. J. Zou, D. W. Li, and R. H. Qu *et al*., "Advanced High Torque Density PM Vernier Machine with Multiple Working Harmonics," *IEEE Trans. on Ind. Appl*., vol. 53, no. 6, pp. 5295–5304, Nov.-Dec. 2017.

[13] Y. L. Yu, F. Chai, and Y. L. Pei *et al*., "Comparisons of Torque Performance in Surface-mounted PM Vernier Machines with Different Stator Tooth Topologies," *IEEE Trans. on Ind. Appl.*, vol. 55, no. 4, pp. 3671–3684, Jul.-Aug. 2019.

[14] L. Xu, G. H. Liu, and W. X. Zhao *et al*., "Hybrid Stator Design of Fault-tolerant Permanent-magnet Vernier Machines for Direct-drive Applications," *IEEE Trans. on Ind. Electron.*, vol. 64, no. 1, pp. 179–190, Jan. 2017.

[15] Y. Zhao, D. W. Li, and Z. Y. Liang *et al*., "A High Power Factor PM Vernier Machine with Segmented Stator," *IEEE Trans. on Transport. Electrific.*, vol. 10, no. 4, pp. 9294–9303, Dec. 2024.

[16] G. H. Xu, W. X. Zhao, and G. H. Liu *et al*., "Torque Performance Improvement of Consequent-pole PM Motors with Hybrid Rotor Configuration," *IEEE Trans. on Transport. Electrific.*, vol. 7, no. 3, pp. 1561–1572, Sept. 2021.

[17] T. G. Wang, X. Y. Zhu, and Z. X. Xiang *et al*., "Improvement of Power Factor and Torque of a PM Vernier Motor from Perspective of Armature and PM Field Harmonics," *IEEE Trans. on Transp. Electrific.*, vol. 10, no. 3, pp. 6064–6075, Sept. 2024.

[18] M. Cheng, W. Hua, and J. Z. Zhang *et al*., "Overview of Stator-permanent Magnet Brushless Machines," *IEEE Trans. on Ind. Electron.*, vol. 58, no. 11, pp. 5087–5101, Nov. 2011.

[19] Y. Meng, X. Y. Yang, and H. Chen *et al*., "Design and Analysis of a New Hybrid-excited Flux Switching Machine with Dual-set of PMs," *IEEE Trans. on Ind. Electron.*, vol. 73, no. 1, pp. 1110–1121, Jan. 2026.

[20] Y. Meng, S. H. Fang, and Y. Z. Zhu *et al*., "Surrogate-model-based Multilevel Optimization Design and Analysis of a New Flux Switching Machine with Double-sided PM Excitation," *IEEE Trans. on Transport. Electrific.*, vol. 10, no. 4, pp. 10136–10146, Dec. 2024.

[21] A. Ghaheri, A. Zarghani, and E. Afjei *et al*., "A Detailed Thermal Analysis for Performance Improvement of Axial Transverse-flux-switching PM Wind Turbine Generator," *CES Trans. on Electr. Mach. and Syst.*, vol. 9, no. 2, pp. 212–223, Jun. 2025.

[22] H. Hua, H. R. Ge, and Z. Q. Zhu *et al*., "Torque Improvement and Magnet Reduction of Flux Reversal Permanent Magnet Machines," *IEEE Trans. on Energy Convers.*, vol. 40, no. 3, pp. 1798–1809, Sept. 2025.

[23] L. N. Jian, Y. J. Shi, and C. Liu *et al*., "A Novel Dual-permanent-magnet-excited Machine for Low-speed Large-torque Applications," *IEEE Transactions on Magnetics*, vol. 49, no. 5, pp. 2381–2384, May 2013.

[24] H. Chen, D. W. Li, and Y. Meng *et al*., "Investigation of a Novel Dual-side PM Vernier Machine with Two-slot-pitch Coils," *IEEE Trans. on Transp. Electri.*, vol. 11, no. 1, pp. 2108–2119, Feb. 2025.

[25] Y. Meng, S. H. Fang, and Y. Li *et al*., "Design and Analysis of New Dual-stator Flux Modulated Machines with Dual-PM Excitation," *IEEE Trans. on Ind. Appl.*, vol. 59, no. 2, pp. 1383–1393, Mar.-Apr. 2023.

[26] Y. Li, H. Yang, and H. Y. Lin *et al*., "Torque Generation Mechanism and Performance Evaluation of a Dual-sided PM Machine with Stator U-shaped Magnets," *IEEE Trans. on Ind. Appl.*, vol. 58, no. 1, pp. 250–260, Jan.-Feb. 2022.

[27] Y. T. Gao, T. Kosaka, and Y. Liu *et al*., "Comparative Analysis of Double Flux Modulation Permanent Magnet Machines with Different Stator PM Arrangements," *IEEE Trans. on Ind. Appl.*, vol. 58, no. 2, pp. 1941–1951, Mar.-Apr. 2022.

[28] Q. S. Wang, S. X. Niu, and L. Yang, "Design Optimization and Comparative Study of Novel Dual-PM Excited Machines," *IEEE Trans. on Ind. Electron*., vol. 64, no. 12, pp. 9924–9933, Dec. 2017.

[29] Y. M. Shen, X. H. Zhu, and H. Yang *et al*., "Design and Evaluation of Dual Excitation Permanent Magnet Linear Machine with Optimal Utilization of Extended Working Harmonics," *IEEE Trans. on Ind. Electron.*, vol. 72, no. 11, pp. 11647–11659, Nov. 2025.

[30] H. Chen, Y. Meng, and Q. Zhang *et al*., "Design and Analysis of a New Asymmetric Consequent-pole Flux Reversal Dual-PM Excited Machine with Trapezoidal PMs," *IEEE Trans. on Transp. Electr.*, vol. 11, no. 4, pp. 8702–8713, Aug. 2025.

[31] H. Chen, Y. Meng, and B. Y. Li *et al*., "Power Factor Enhancement Mechanism of an Asymmetric Consequent-pole Flux Reversal Dual-PM Excited Machine," *IEEE Trans. on Transp. Electr*., Early Access, pp. 1–1.

[32] L. Xu, Z. Y. Chen, and W. X. Zhao *et al*., "Analysis of a Fault-tolerant Dual-permanent-magnet Vernier Machine with Hybrid Stator," *IEEE Trans. on Transp. Electrif.*, vol. 10, no. 3, pp. 6559–6570, Sept. 2024.

[33] F. R. Wei, Z. Q. Zhu, and H. Qu *et al*., "New Dual-PM Spoke-type Flux-reversal Machines for Direct-drive Applications," *IEEE Trans. on Ind. Appl*., vol. 58, no. 5, pp. 6190–6202, Sept.-Oct. 2022.

[34] K. F. Xie, D. W. Li, and R. H. Qu *et al*., "A Novel Permanent Magnet Vernier Machine with Halbach Array Magnets in Stator Slot Opening," *IEEE Trans. on Magn.*, vol. 53, no. 6, pp. 1–5, Jun. 2017.

[35] W. X. Zhao, Q. Z. Hu, and J. H. Ji *et al*., "Torque Generation Mechanism of Dual-permanent-magnet-excited Vernier Machine by Air-gap Field Modulation Theory," *IEEE Trans. on Ind. Electron.*, vol. 70, no. 10, pp. 9799–9810, Oct. 2023.

Hong Chen (Member, IEEE) was born in Shandong, China. She received the B.E. degree from the Wuhan University of Technology, Wuhan, China, in 2010, and the Ph.D. degree from the Huazhong University of Science and Technology, Wuhan, China, in 2015, both in electrical engineering. She is currently a Lecturer with the College of Electrical Engineering and Automation, Shandong University of Science and Technology. Her research interests include the design of permanent magnet machines and special electrical machines.

Yao Meng (Member, IEEE) received the B.Eng. degree in electrical engineering and automation from Qingdao University of Science and Technology, Qingdao, China, in 2012, the M.Sc. degree in power electronics and drives from the University of Nottingham, Nottingham, UK, in 2013, and the Ph.D. degree in electrical engineering from Southeast University, Nanjing, China, in 2022.

From 2014 to 2017, he was an Engineer with the Research and Development center of CRRC Qingdao Sifang Co., Ltd., Qingdao, China, where his research activities were mainly in the design and research of traction systems of high-speed trains. Since 2023, he has been with Shandong University of Science and Technology, Qingdao, China, where he is currently an associate professor with the College of Electrical Engineering and Automation. His research interests include design and control of permanent magnet machines.

Boyi Li received the B.Eng. degree in mechatronics engineering from Shandong University of Science and Technology, Taian, China, in 2023. He is currently working toward the M.Eng. degree in Electrical Engineering with Shandong University of Science and Technology, Qingdao, China.

His research interests include the design and analysis of permanent magnet machines.

Dawei Li (Senior Member, IEEE) was born in Henan, China. He received his B.E. degree from the Harbin Institute of Technology, Harbin, China, in 2010 and his Ph.D. degree from the Huazhong University of Science and Technology, Wuhan, China, in 2015, both in electrical engineering.

In 2015, he joined the Huazhong University of Science & Technology, Wuhan, China. He has authored more than 60 published technical papers and is the holder of more than 10 patents/patent applications. His research interests include the design and analysis of flux-modulation permanent-magnet brushless machines.

Dr. Li received the 2016 Best Poster Presentation Award from the XXIIth International Conference on Electrical Machines (2016) and Hubei Province Excellent Doctoral Dissertation (2016), China.

Ronghai Qu (Fellow, IEEE) received the B.E. and M.S. degrees from Tsinghua University, Beijing, China, in 1993 and 1996, respectively, and the Ph.D. degreefrom the University of WisconsinMadison, Madison, USA, in 2002, all in electrical engineering.

He is currently the Director of the State and Province Joint Engineering Research Center of Novel Electrical Machines, and the Director of the Center for Advanced Electrical Machines and Drives (CAEMD), Wuhan, China. He was a Senior Electrical Engineer with the Electrical Machines and Drives Laboratory, General Electric (GE) Global Research Center, Niskayuna, NY, USA, from 2003 to 2010. In 2010, he joined Huazhong University of Science & Technology, Wuhan, China. From 2012 to 2016, he served as the Deputy Dean of the School of Electrical & Electronic Engineering, Huazhong University of Science & Technology, Wuhan, China. His research interests include design and drive of electrical machines. He has published over 400 technical papers including 14 IEEE award papers and holds over 170 patents.